Nuclear Instruments and Methods in Physics Research A 670 (2012) 32–39

Contents lists available at SciVerse ScienceDirect

Nuclear Instruments and Methods in Physics Research A

journal homepage: www.elsevier.com/locate/nima

The use of the gas-filled magnet technique for the detection of medium mass ions

J.M. Figueira [a,b,c,*], K.E. Rehm [c], C.M. Deibel [c,d], J.O. Fernández Niello [a,e], J. Greene [c], C.L. Jiang [c], H.Y. Lee [c], S.T. Marley [c,f], R.C. Pardo [c], N. Patel [c,g], M. Paul [h], C. Ugalde [c], G. Zinkann [c]

[a] Laboratorio Tandar, Comisión Nacional de Energía Atómica, B1650KNA San Martín, Buenos Aires, Argentina
[b] Consejo Nacional de Investigaciones Científicas y Técnicas, C1033AAJ Buenos Aires, Argentina
[c] Physics Division, Argonne National Laboratory, Argonne, IL 60439, USA
[d] Joint Institute for Nuclear Astrophysics, Michigan State University, East Lansing, MI 48824, USA
[e] Escuela de Ciencia y Tecnología, Universidad de San Martín, B1650BWA San Martín, Buenos Aires, Argentina
[f] Physics Department, Western Michigan University, Kalamazoo, MI 49008, USA
[g] Department of Physics, Colorado School of Mines, Golden, CO 80401, USA
[h] Racah Institute of Physics, Hebrew University, Jerusalem, Israel

ARTICLE INFO

Article history:
Received 18 October 2011
Accepted 9 December 2011
Available online 21 December 2011

Keywords:
Charged-particle spectroscopy
Gas-filled magnet technique
(α,p) reactions
(p,α) reactions
X-ray bursts

ABSTRACT

The use of the gas-filled magnet technique for the detection of intermediate mass ($A\sim$ 20–40) recoil nuclei produced in (p,α) reactions in inverse kinematics has been investigated. Through a series of calibration measurements with ^{27}Al, ^{28,29}Si and ^{33}S beams the optimum parameterization for calculating the average charge-state distribution in a gas-filled magnet has been determined. By measuring the magnetic rigidity, the time-of-flight and the differential energy loss of the particles at the focal plane of a gas-filled Enge Split Pole spectrograph it was possible to separate and identify the (p,α) reaction products from elastically scattered particles at very small scattering angles. This technique was then tested by measuring the p(^{33}S,^{30}P)α and p(^{37}K,^{34}Cl)α reactions.

1. Introduction

With the advent of radioactive ion beams many new questions in nuclear structure and nuclear astrophysics can be addressed. When compared to measurements with stable beams, however, experiments induced by radioactive beams suffer from three difficulties: (1) low beam intensities, (2) large kinematic shifts, which occur through the use of inverse reaction kinematics (i.e., heavier beams bombarding lighter targets), and (3) contaminants from neighboring elements or isotopes which are often present in radioactive ion beams (so-called 'cocktail beams'). To eliminate some of these difficulties next-generation radioactive beam facilities with higher beam intensities are being built and new spectrometers optimized for inverse kinematic reactions have been developed. This paper describes a method to address the difficulties that arise by using 'cocktail beams', through the identification of the heavy reaction products and beam components with respect to mass and/or nuclear charge at very small scattering angles.

The use of inverse kinematics in studies with radioactive beams results in the beam-like reaction products being emitted at small angles. For some studies, such as measurements of (p,α) reactions, these products need to be separated from more abundant scattered beam particles. In experiments involving beams up to about mass 20 (e.g., p(^{17}F,α)^{14}O [1]), where the opening angles for the beam-like particles are $\theta_{lab} \geq 6.5^{\circ}$, Si-strip detectors can be used for detecting and identifying the outgoing particles. However, in experiments involving heavier beams (e.g., ^{4}He(^{44}Ti,p)^{47}V [2]), the opening angles are smaller and recoil separators have to be employed. While this technique provides excellent mass and *Z*-identification the fact that only one charge state could be measured in the focal plane reduced the detection efficiency by a factor of about 5. In the intermediate-mass regime, $A\sim 20-40$, a new technique has been developed to address this challenge which is the subject of this paper.

Reactions in the intermediate-mass region are of interest to nuclear astrophysics for studies of novae and X-ray bursts (XRB), thermonuclear explosions occurring on the surfaces of white dwarf and neutron stars, respectively. Specifically in XRBs, the nuclear flow is driven by the triple-α reaction, the rapid proton capture process (rp-process) and the αp-process toward the proton-drip line [3]. The αp-process, which occurs in the $A\sim$ 20–40 region, is strongly temperature dependent due to the large Coulomb barriers involved. As a result, the cross sections

* Corresponding author at: Laboratorio Tandar, Comisión Nacional de Energía Atómica, B1650KNA San Martín, Buenos Aires, Argentina. Fax: +54 11 6772 7121.
E-mail address: figueira@tandar.cnea.gov.ar (J.M. Figueira).

0168-9002/$ - see front matter © 2011 Elsevier B.V. All rights reserved.
doi:10.1016/j.nima.2011.12.048

and the related reaction rates can have a large effect on nucleosynthesis in XRBs as shown in a recent sensitivity study [4]. Specifically, (α,p) reactions on intermediate-mass waiting points (e.g., ^{22}Mg, ^{26}Si, ^{30}S, and ^{34}Ar) may significantly affect XRB nucleosynthesis and the resulting light curves [5]. However, these reactions have not been studied extensively in the laboratory, since beams of these short-lived nuclei with sufficient intensity are not yet available. In order to measure these reaction rates (or to get at an upper limit) we have started measurements of the time-inverse (p,α) reactions on ^{25}Al, ^{29}P, ^{33}Cl, and ^{37}K using radioactive beams and have thus developed a method to address the challenges involved in these types of experiments.

These secondary ^{25}Al, ^{29}P, ^{33}Cl, and ^{37}K beams are produced via the (d,n) reaction at the ATLAS In-Flight facility by bombarding a deuterium gas targets with stable beams of ^{24}Mg, ^{28}Si, ^{32}S, and ^{36}Ar, respectively [6]. These secondary beams, however, can have considerable contaminations from the stable primary beams and it is necessary to measure the outgoing α particles in coincidence with the residual heavy nuclei (e.g., ^{34}Ar for the ^{37}K(p,α)^{34}Ar reaction [7]). As maximum emission angles of the heavy beam-like nuclei are approximately 2.7°–3.1°, Si strip detectors cannot be employed. We have, therefore, studied the possibility of using a magnetic spectrometer operating in the so-called gas-filled magnet (GFM) mode for detecting the medium-mass recoil particles at very small scattering angles. In order to test this technique we have first used beams of stable nuclei (^{27}Al, ^{28,29}Si and ^{33}S). The ^{33}S beam was then used for a first measurement of the p(^{33}S,α)^{30}P reaction, followed by a similar experiment with a low-intensity radioactive ^{37}K beam.

The principle of the GFM technique will be described in Section 2. The split-pole spectrograph and its focal plane detector system which have been used in these experiments are explained in Section 3. The results obtained with medium mass ion beams are presented in Section 3. Possible applications for a study of deep-inelastic reactions and a summary are given in Sections 4 and 5, respectively.

2. The gas-filled magnet technique

The GFM technique was originally developed by Fulmer and Cohen [8,9] for the separation of fission fragments and further refined by Armbruster and collaborators [10–12]. It has been used in studies of heavy element production [13–16], for isobar separation in accelerator mass spectrometry [17–20], in sub-barrier fusion reactions in direct and inverse kinematics [21–23], and for the identification of light ions in (p,α) reactions [24]. In the present work we apply the GFM method for the first time to the identification of medium mass ions in measurements of (p,α) reactions of astrophysical interest.

Ions of mass m and velocity v passing through a target foil emerge with a distribution of ionic charge states q [25]. In vacuum these ions move in a magnetic field on circular trajectories whose radii ρ are given by the expression:

$$B\rho = \frac{mv}{qe} \quad (1)$$

where q is the charge state of the ion, B is the strength of the magnetic field and e is the elementary charge. Hence, nuclei of the same atomic number Z, mass number A and energy E but with different charge states q will follow different trajectories which are spatially distributed at the focal plane as shown in Fig. 1(a). If the magnetic field region is filled with a gas at low pressure ($\sim$10 Torr), the incident ions collide with the gas atoms along their trajectories, causing the charge state of the ions to fluctuate due to electron capture and loss processes. If the number of collisions is high enough ($\gtrsim 10^4$, depending on the gas pressure

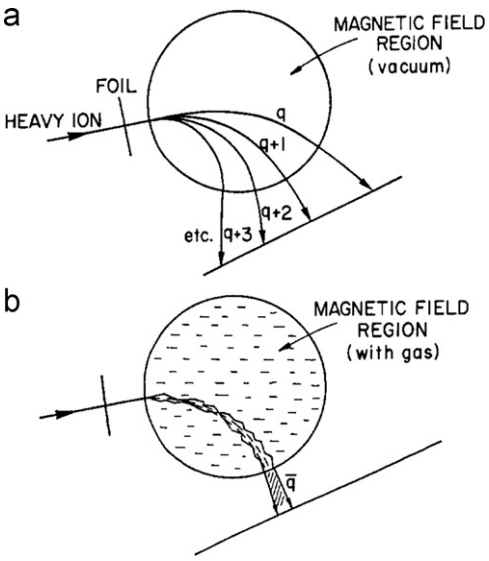

Fig. 1. Schematic illustration of the trajectories followed by nuclei of the same Z, A and E but different charge states q in a magnetic field region: (a) in vacuum; (b) filled with gas. In vacuum, ions with different charge states will have different radii of curvature. In a gas-filled region, the ions will have curvatures $\overline{\rho}$ controlled by the mean charge state $\overline{q}$ and the average velocity $\overline{v}$. Taken from Ref. [27].

and the collision cross sections), the average trajectory is determined by a mean charge state $\overline{q}$ and an average velocity $\overline{v}$. Therefore, the particles will follow a trajectory with a radius $\overline{\rho}$, given by $B\overline{\rho} = m\overline{v}/(\overline{q}e)$, as is schematically represented in Fig. 1(b). Various semi-empirical parameterizations have been derived for the calculation of $\overline{q}$ which are summarized in Refs. [25,26] and are discussed in more detail in Section 3.1. If particles with similar velocities enter the magnetic field, the average charge state $\overline{q}$ is in first order given by $\overline{q} \propto v/Z^{\alpha}$ with $\alpha \sim 0.4$. Thus, a gas-filled magnet disperses these particles in the focal plane according to $m/Z^{0.4}$. Ions with different atomic numbers Z have different path lengths and specific energy losses which results in a different time-of-flight between target and focal plane detector. In a plot of time-of-flight vs magnetic rigidity these different ions end up in different 'islands' as shown, e.g., in Fig. 4 of Ref. [24].

For the detection of the heavy recoils from (p,α) reactions in inverse-kinematics the GFM method provides two advantages. All charge states of the same nuclear species converge into one group at the focal plane, thus increasing the detection efficiency which is essential for low-intensity radioactive beam experiments. Moreover, the magnetic rigidities of the beam particles and some of the heavy reaction products of interest are sufficiently different to result in a spatial separation of both groups in the focal plane. Therefore, through a proper selection of the magnetic field and/or partial shielding of the focal plane it is possible to focus the reaction products of interest onto the focal plane without detecting the beam particles, thereby avoiding prohibitively high counting rates.

A schematic of the setup used in the (p,α) experiments is shown in Fig. 2. The α particles from the (p,α) reaction are detected in an annular Si strip detector whose front side is divided into concentric rings and mounted coaxially with the beam, so that the azimuthal symmetry of the reaction can be exploited. The correlated heavy reaction products emitted at forward angles are detected in coincidence with these α particles using the gas-filled spectrograph. Since the incident beam has to pass through a pressure foil at the entrance of the magnet the beam intensity has to be kept below 10^7 particles/s in order to avoid breakage.

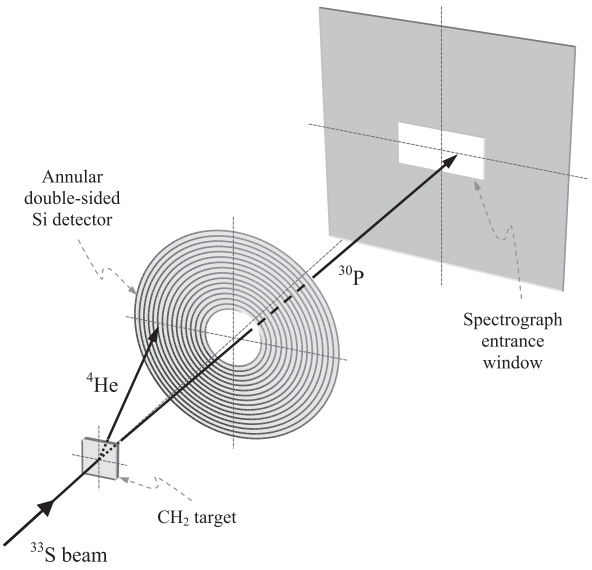

Fig. 2. A schematic of the experimental setup.

3. Test experiments with medium mass nuclei

The experiments described below were performed at the ATLAS facility at Argonne National Laboratory. An Enge split-pole magnetic spectrograph filled with N_2 gas at pressures between 10 and 20 Torr was used to momentum analyze the heavy residual nuclei at forward angles. While hydrogen or helium would have been a better choice for the gas-filled magnet due to their lower charge, safety concerns, the need of higher pressures and the existing cryo and sorption pumping system at the spectrograph prevented the use of these gases.

Although not originally built as a gas-filled recoil separator the split-pole spectrograph is, due to its moderate dispersion, very well suited for the separation and detection of heavy ions. The spectrograph has a maximum solid angle of ~ 5 msr and accepts particles in the angular range $\delta\theta = \pm 3.85^\circ$. In the focal plane the particles are detected by a hybrid x–y-position sensitive detector system. It consists of a 5-cm thick x–y-position sensitive Parallel-Grid Avalanche Counter (PGAC) filled with isobutane at a pressure of 3–5 Torr [21] followed by a 30 cm deep multi-anode Ionization Chamber (IC) which is separated from the PGAC by a 6.25 μm mylar foil and filled with CF_4. The active area of the focal plane counter is 10×48 cm^2. Because of the large area of the window separating the IC from the PGAC the pressure in the IC has to be kept below 20 Torr. In addition to the x–y position information the PGAC provides also a fast timing signal which, together with the signal from the pulsed beam allows a determination of the time-of-flight from the target to the focal plane. The electric field in the IC is perpendicular to the path of the incoming particle, which minimizes the drift time of the electrons and ions. The anode is subdivided in several strips allowing us to measure multiple ΔE signals for additional particle identification. This detector system has been used in the past for measurements of evaporation residues from heavy-ion induced fusion reactions [21] and more details of the detector can be found in this reference.

3.1. GFM calibration runs

In order to obtain a better understanding of the energy and Z-dependence of the average charge state $\overline{q}$, a series of calibration runs were performed by bombarding a Au target with ion beams of ^{27}Al, ^{28}Si and ^{29}Si at $E = 10$ MeV/nucleon and detecting elastically scattered particles at $\theta_{lab} = 2^\circ$. The results of these test runs were then compared to simulations carried out with the code RAYTRACE-GFM [27–29] which calculates the transport of ions in a gaseous medium. The mean values of focal-plane positions $\overline{X}$ and time-of-flights $\overline{TOF}$ as function of the field strength B obtained for the three beams are shown in Fig. 3(a) by the open and full symbols, respectively. The solid, dashed and dotted lines exhibit the results of the RAYTRACE-GFM calculations which are discussed below.

The RAYTRACE-GFM code calculates trajectories of heavy ions traveling through different types of ion-optical devices (dipoles, multipoles, electrostatic deflectors, velocity filters, solenoids, etc.) when filled with low-pressure gas. For our case, using the detailed configuration of the magnetic field regions of the Enge split-pole spectrograph, the trajectories are calculated [17] by integrating

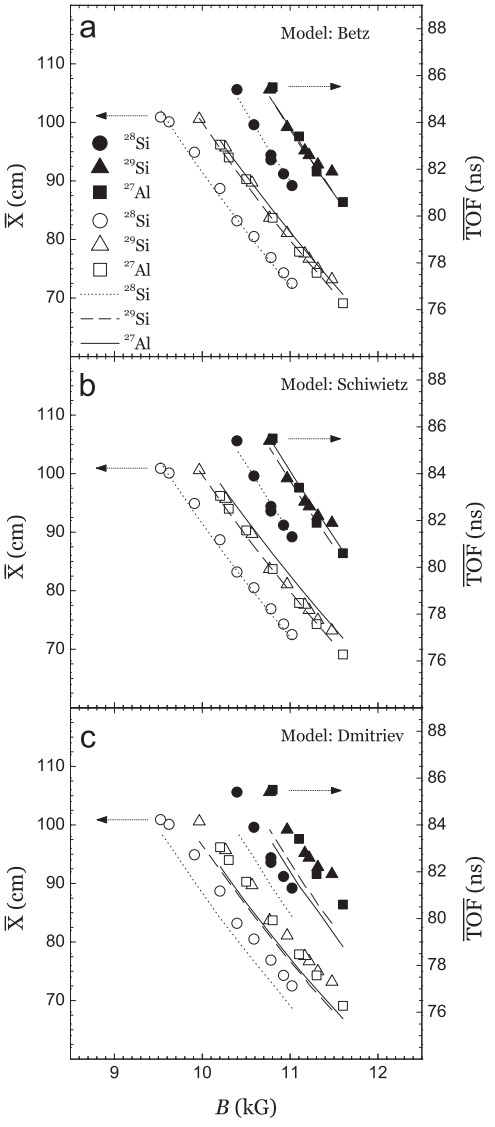

Fig. 3. Mean values of focal-plane position (open symbols, left scale) and time-of-flight distributions (solid symbols, right scale) plotted as a function of the magnetic field. Experimental results (symbols) and calculations (solid, dashed and dotted lines) are presented for three different beams: ^{27}Al (squares and solid line), ^{28}Si (circles and dotted line) and ^{29}Si (triangles and dashed line). Panels (a)–(c) correspond to calculations done using the Betz, Schiwietz and Dmitriev charge state distributions, respectively.

the equation of motion of the ions:

$$\frac{d(m\boldsymbol{v})}{dt} = q(\boldsymbol{B}\times\boldsymbol{v}) - \frac{dE}{dx}\frac{\boldsymbol{v}}{v}. \quad (2)$$

The simulation of the ion–gas interaction process is performed with a standard Monte Carlo method, using a Gaussian-shaped equilibrium charge-state distribution:

$$F_q = \frac{1}{d\sqrt{2\pi}}\exp\left(-\frac{(q-\overline{q})^2}{2d^2}\right) \quad (3)$$

where $\overline{q}$ is the average charge state and d is the standard deviation of the distribution.

Different semi-empirical parameterizations for $\overline{q}$ and d can be chosen for the calculations. Among them are

(i) the Betz parameterization [25,30,31]

$$\overline{q} = Z\left[1 - C\exp\left(A\frac{(v/v_0)^{\delta}}{Z^{\gamma}}\right)\right] \quad (4)$$

$$d = d_1 Z^{w} \quad (5)$$

where $C=1$, $A=0.555$, $\delta=1.175$, $\gamma=0.607$, $d_1=0.27$ and $w=0.5$ are parameters evaluated from experimental data in nitrogen gas and $v_0 = 2.19\times10^6$ m/s is the Bohr velocity;

(ii) the Dmitriev–Nikolaev parameterization [32]

$$\overline{q} = Z\left[\frac{\log((v/v_0)Z^{\alpha_1}/m_1)}{\log(n_1 Z^{\alpha_2})}\right] \quad (6)$$

$$d = d_1 Z^{w}, \quad (7)$$

with $\alpha_1=0.4$, $\alpha_2=0.3$, $m_1=0.41$, $n_1=7$, $d_1=0.32$ and $w=0.45$ in nitrogen gas; and

(iii) the Schiwietz parameterization [33]

$$\overline{q} = Z\frac{376x + x^6}{1428 - 1206x^{0.5} + 690x + x^6} \quad (8)$$

with

$$x = (v/v_0 Z^{-0.52} Z_{gas}^{0.03-0.017Z^{-0.52}v/v_0})^{1+0.4/Z} \quad (9)$$

and

$$d = \frac{0.7}{Z^{-0.27} Z_{gas}^{0.035-0.0009Z} f(\overline{q}) f(Z-\overline{q})} \quad (10)$$

with

$$f(x) = \sqrt{(x + 0.37Z^{0.6})/x}. \quad (11)$$

The last parameterization has recently been incorporated into the code for experiments with medium-mass nuclei.

The lines in Fig. 3 are RAYTRACE-GFM calculations of $\overline{X}$ and $\overline{TOF}$, for ^{27}Al (solid), ^{28}Si (dotted) and ^{29}Si (dashed). Panels (a)–(c) correspond to the Betz, Schiwietz and Dmitriev models for the charge state distributions. As can be seen from Fig. 3 the calculations using the Betz and Schiwietz parameterizations are in very good agreement with the experimental results, while the calculations of both $\overline{X}$ and $\overline{TOF}$ for the Dmitriev parameterization are systematically shifted to smaller values. It must be noted, however that the validity of the Dmitriev model covers only the range $0.3 \lesssim \overline{q}/Z \lesssim 0.9$ [32] which translates to a region in projectile velocity equivalent to $2.6 \lesssim v/v_0 \lesssim 13$. At the bombarding energies used in this calibration run (10 MeV/nucleon) the projectile velocity is $v/v_0 = 20$. At these velocities Eq. (6) gives for ^{27}Al $\overline{q}/Z = 1.05$, i.e., an unphysical value. In Eq. (1), this $\overline{q}$ leads to a lower radius and, hence, the mean value of the focal-plane position $\overline{X}$ is shifted towards smaller values. The Betz and Schiwietz parameterizations are valid in the range $v/v_0 \gtrsim 1$ [25,33] which includes the velocities used in this experiment.

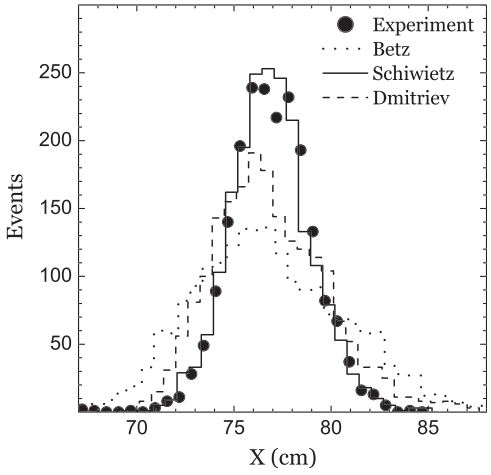

Fig. 4. X distributions, in gas-filled magnet mode, of ^{28}Si particles elastically scattered on a ^{197}Au target at $\theta = 2^{\circ}$, $E = 10$ MeV/nucleon, $P = 15$ Torr and $B = 10.782$ kG. The full symbols are the experimental spectrum, while the dotted, solid and dashed lines correspond to calculations using the Betz, Schiwietz and Dmitriev charge state distributions, respectively. The distributions were normalized to have the same number of counts as the experimental spectrum. Only the width obtained with the Schiwietz charge state distribution agrees with the data.

A closer inspection of Fig. 3 shows that the centroids in the X and TOF distributions, in particular the overlap between the ^{27}Al and ^{29}Si data, are better described by the Betz parameterization. For that reason we have chosen this parameterization (given by Eq. (4)) for $\overline{q}$ in the RAYTRACE-GFM calculations explained below.

Another important input for the RAYTRACE-GFM calculations are the variances of the X and TOF parameters. Since no rebunching resonator was used in these experiments a variance, σ, of 1 ns was assumed for the width of the time distribution. The width of the X distribution is dominated by the width of the q distribution which can be calculated from the parameters d in Eqs. (5), (7) and (10). A comparison of the experimental data for ^{28}Si with the predictions of Betz, Dimitriev and Schiwietz is shown in Fig. 4. In this comparison it has to be kept in mind that the widths depend on many parameters, e.g., the stopping gas, the type of ion, etc. A detailed comparison of the various formulas is beyond the scope of this paper. However, for the ions studied in this work the parameterization of Schiwietz gives the best agreement with the experimental data and is therefore adopted in the subsequent analysis.

Fig. 5 shows a comparison of the experimental results for the two-dimensional spectra of TOF vs X and the predictions from RAYTRACE-GFM using the Betz parameterization for the mean charge state $\overline{q}$ and the Schiwietz parameterization for the width parameter d (Betz–Schiwietz model), for the ^{27}Al, ^{28}Si and ^{29}Si beams. With the exception of the tails towards longer flight times in the experimental spectrum, which are caused by the finite TOF acceptance of the accelerator, good agreement with the theoretical predictions is obtained.

3.2. Study of the ^{33}S(p,α)^{30}P reaction with a stable ^{33}S beam

After these calibration runs with ^{27}Al, ^{28}Si and ^{29}Si beams the p(^{33}S,^{30}P)α reaction was studied, using a stable ^{33}S beam incident on a 360 μg/cm^2 CH_2 target. Fig. 6 shows the kinematic correlation between detection angle and energy of the α particles and the ^{30}P reaction products calculated for a ^{33}S bombarding energy of 179 MeV. Because of the choice of inverse kinematics the kinematic curves have both a low and a high energy solution at each angle. Small center-of-mass angles correspond to the high-energy part of the heavy recoils (i.e., to the low-energy solution

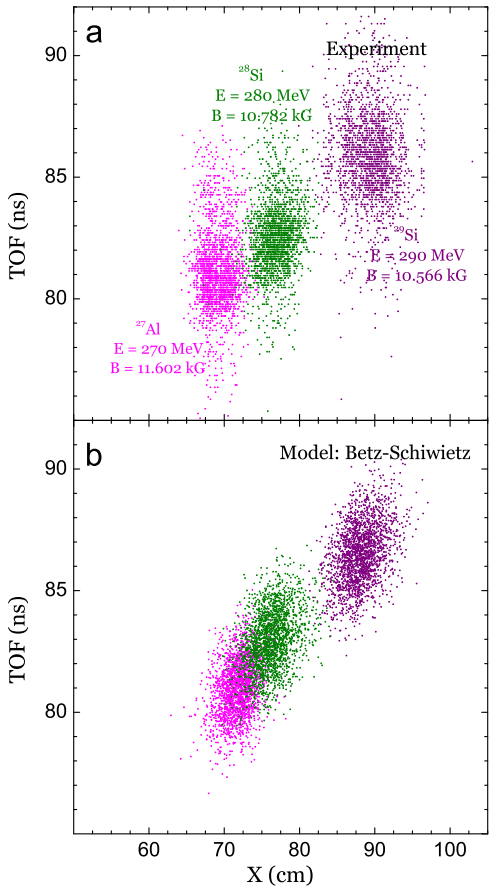

Fig. 5. (Color online) Scatter plots of events in the TOF vs X plane for ^{27}Al, ^{28}Si and ^{29}Si ions detected in the gas-filled split-pole spectrograph. Panel (a): superposition of three experimental spectra, taken from ^{27}Al, ^{28}Si and ^{29}Si elastically scattered from a ^{197}Au target at $\theta = 2^\circ$, $E = 10$ MeV/nucleon, $P = 15$ Torr and $B = 11.602$, 10.782 and 10.566 kG, respectively. Panel (b): RAYTRACE-GFM calculations using the Betz parameterization for the mean charge state $\bar{q}$ and the Schiwietz parameterization for the width parameter d (model Betz–Schiwietz), for the same particle groups and the same conditions as in panel (a). The calculations reproduce the separation along the focal plane and the time of flight obtained experimentally.

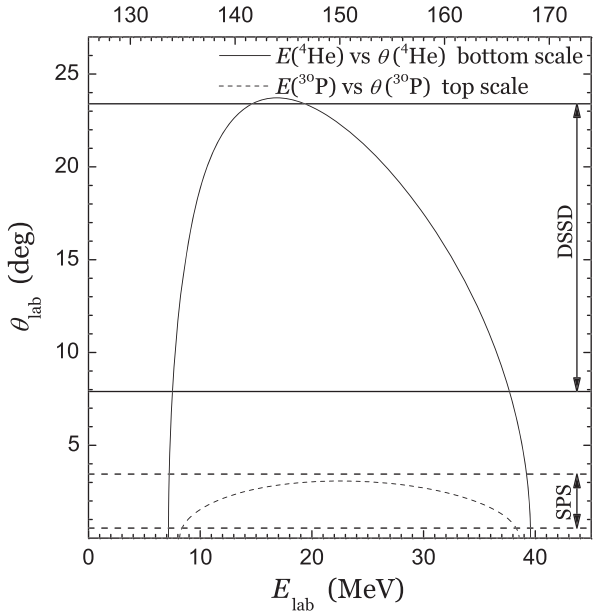

Fig. 6. Kinematic relations between detection angle and energy for the products of the p(^{33}S,^{30}P)α reaction at a bombarding energy of 179 MeV. Acceptance limits of the DSSD and PGAC are indicated by the solid and dashed horizontal lines, respectively.

for the α's). As can be seen from Fig. 6, the α particles are restricted to a cone with an opening angle of $\sim 24^\circ$, while the heavy reaction products ^{30}P are more forward peaked with a maximum angle of $\sim 3.1^\circ$. The acceptance limits of the annular Si-detector and the split-pole spectrograph are indicated by the solid and dashed horizontal lines, respectively. Since the intensity of the stable ^{33}S beam exceeded 10^7 particles/s, the spectrograph was moved away from 0° and the majority of the ^{33}S beam was stopped before the entrance foil of the GFM. The angular range covered with the GFM was $\theta_{lab} = 0.5^\circ - 3.5^\circ$. Within the acceptance range of the Si detector, $\theta_{lab} = 7.9^\circ - 23.4^\circ$, the energies of the corresponding ^{30}P particles range from 136.6 to 166.8 MeV. With this information RAYTRACE-GFM calculations were performed in order to predict where the ^{30}P reaction products and the elastically scattered ^{33}S particles would appear in the focal plane. Due to a problem with the time-to-amplitude converter no TOF signal was available during this run. Since the focal plane detector in the spectrograph can also provide an energy-loss signal from the ionization chamber we have calculated a spectrum of ΔE vs X (Fig. 7(b)). An experimental spectrum of the same parameters is shown in Fig. 7(a). This spectrum is found to be in good agreement with the RAYTRACE-GFM predictions. Requiring a coincidence between a Si detector event, a GFM event and restricting the particles to the ^{30}P region in Fig. 7(b) in the off-line analysis produces the spectrum shown in Fig. 8 for an incident energy of 179 MeV. The solid line is the kinematic curve for population of the ground state, while the three subsequent dotted lines represent transitions to the first three excited states in ^{30}P. The events corresponding to the ground state transition of the ^{33}S(p,α)^{30}P reaction are clearly identified. This result confirms that the GFM technique presented here can be applied successfully to the identification of (p,α) reaction in the mass 20–40 range. The vertical lines at low energies in Fig. 8 correspond to inelastic excitations of ^{33}S from the p(^{33}S,p)^{33}S′ reaction which are present as a background in Fig. 7(b). From these spectra angular distributions of the α particles can be obtained, which, after integration, result in cross sections of the ^{33}S(p,α)^{30}P reaction [34].

3.3. Study of the ^{37}K(p,α)^{34}Ar reaction with a radioactive ^{37}K beam

Following this 'proof of principle' test of the GFM technique with a stable ^{33}S beam a similar measurement of the ^{37}K(p,α)^{34}Ar reaction with a radioactive ^{37}K ($t_{1/2} = 1.22$ s) beam was performed. The secondary beam was produced via the d(^{36}Ar,^{37}K)n reaction by bombarding a cryogenically cooled gas cell filled with 1.4 atm of deuterium with a 360-MeV beam of ^{36}Ar obtained from the ATLAS accelerator [6]. The ^{37}K particles were separated from the primary ^{36}Ar beam using a 22° bending magnet which was set to transport the ^{37}K^{19+} ions to the target. The majority of the fully stripped primary beam ^{36}Ar^{18+} has a higher magnetic rigidity and is therefore not transmitted. However, energy-degraded ^{36}Ar^{18+} ions will fall into the acceptance window of the bending magnet and will also be transported to the target, although with a different time of flight. In order to eliminate some of these background events, an RF-sweeper has been installed in the beam line [35]. The RF phase was set to let the particles of interest ^{37}K^{19+} pass through the RF-sweeper while the slower ^{36}Ar^{18+} ions experience a vertical deflection and are stopped on a pair of slits located downstream of the sweeper. The intensity of the radioactive beam on target was typically 5×10^4 ^{37}K/s.

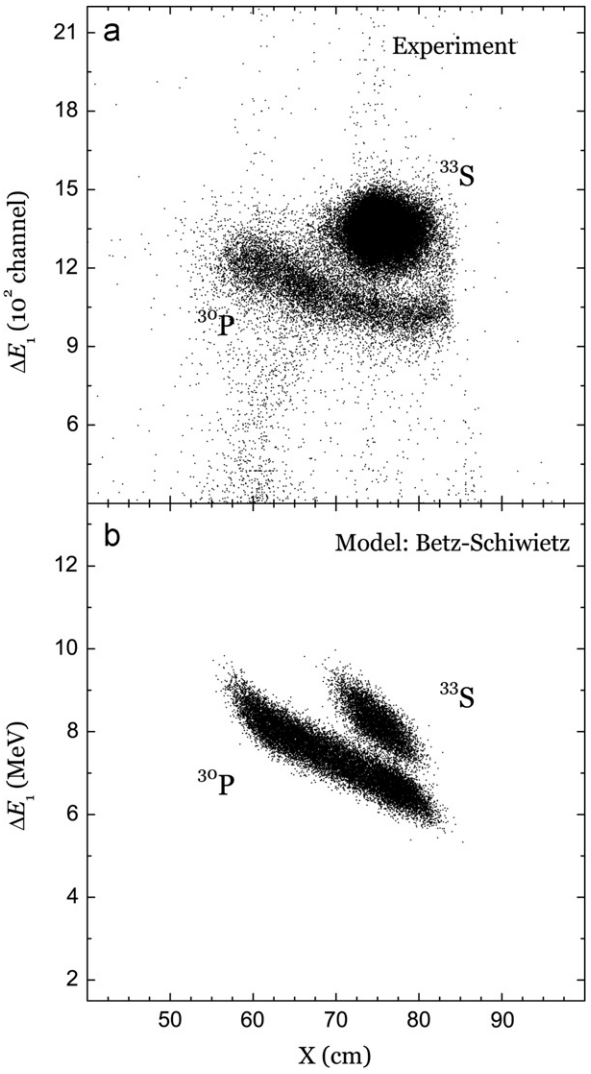

Fig. 7. (a) Experimental spectrum of energy loss in the first anode (ΔE_1) of the ionization chamber vs position at the focal plane detector for the p(^{33}S,α)^{30}P reaction at a bombarding energy of 202 MeV. (b) Spectrum calculated with the code RAYTRACE-GFM for the same experimental conditions. The spectra show the separation of the particles of interest that can be achieved with the GFM technique.

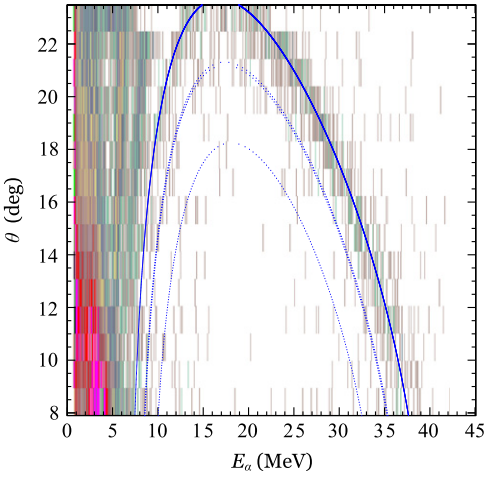

Fig. 8. (Color online) Two-dimensional spectrum of angle vs energy of α particles detected in the DSSD, in coincidence with events in the ^{30}P island at a bombarding energy of 179 MeV. The θ binning represents the angular range covered by each DSSD ring. The lines are calculations of the ^{33}S(p,α)^{30}P kinematics corresponding to the ground state (solid line) and the first three excited states (dotted lines) of ^{30}P. These results demonstrate that light particles detected in the DSSD follow the kinematic curves of the ^{33}S(p,α)^{30}P reaction in a wide energy range, and confirm that this technique can be applied successfully to measure (p,α) transfer reactions in inverse kinematics.

The experimental setup used in this measurement was the same as the one used in the p(^{33}S,α)^{30}P experiment shown in Fig. 2. Since the beam intensity of the secondary ^{37}K beam was less than 10^5 particles/s the spectrograph could be located at 0° with the ^{37}K/^{36}Ar cocktail beam entering the GFM. The kinematic curves of θ vs E for the (p,α) reaction with a ^{37}K beam are similar to the ones shown in Fig. 6. The angular range of the ^{37}K particles in the laboratory frame is restricted to scattering angles less than 2.9°, i.e., to a region where Si detectors are hard to use. In order to identify the region in a ΔE vs X plot where ^{34}Ar reaction products can be expected RAYTRACE-GFM calculations were performed including elastic scattering events from both, the ^{37}K and ^{36}Ar beams as well as the ^{34}Ar and ^{33}Cl products from the corresponding (p,α) reactions. The energies of the incoming ^{37}K and ^{36}Ar beams were 275 MeV and 254 MeV, respectively. The results for ΔE vs X are shown in the top part of Fig. 9 in comparison with the experimental results (bottom). In order to eliminate tails from the primary beam only events corresponding to the high-energy part of the kinematic curve (see e.g., Fig. 6) are shown in the lower part of Fig. 9. Due to the lower beam intensity of the contaminant ^{36}Ar beam ($\sim$20% that of the radioactive ^{37}K beam) as well as its lower energy the ^{36}Ar(p,α)^{33}Cl reaction had a negligible count rate. In this comparison to Fig. 7 it should kept in mind that the experiment was done with ^{37}K beam intensities that were smaller by 3–5 orders of magnitude than comparable stable beam experiments. Despite the poor statistics the structure of the experimental spectrum is found to be in good agreement with the calculations.

4. Outlook

It has recently been suggested [36] to use the GFM technique as a method to separate reaction products produced in deep-inelastic collisions (DIC) from beamlike particles. The data presented in this study can be used to predict the separation of DIC products from the incident beam using a gas-filled split-pole spectrograph. Since the experiment, described above, used particles in the mass $A=30$–40 region we have restricted the calculations to DIC studies involving similar medium mass nuclei. In the simulations it was assumed that DIC products in the mass range $A\sim20$–40 are produced by bombarding a ^{208}Pb target with a ^{36}S beam at an energy of 250 MeV, i.e., about 50% above the Coulomb barrier. Reaction products in the mass range 30–40 generated in such collisions are emitted at small angles with energies corresponding to their respective Coulomb barriers. Other particles at small scattering angles include elastically scattered beam particles as well as heavy (Pb-like) reaction products from central collisions. Target-like deep-inelastic reaction products can be well separated from the primary ^{36}S beam using the GFM technique. Since the parameterization in this study was developed for medium-mass ions we will in the following concentrate on a discussion of the beam-like deep-inelastic reaction products.

While calculations show an appreciable spatial separation between the beam and the target-like reaction products in the focal plane, there is the possibility to achieve also some particle identification for the light reaction products. A TOF vs X plot was calculated for these particles assuming that the split-pole spectrograph was filled with 15 Torr of N_2. Fig. 10(a) shows the islands in

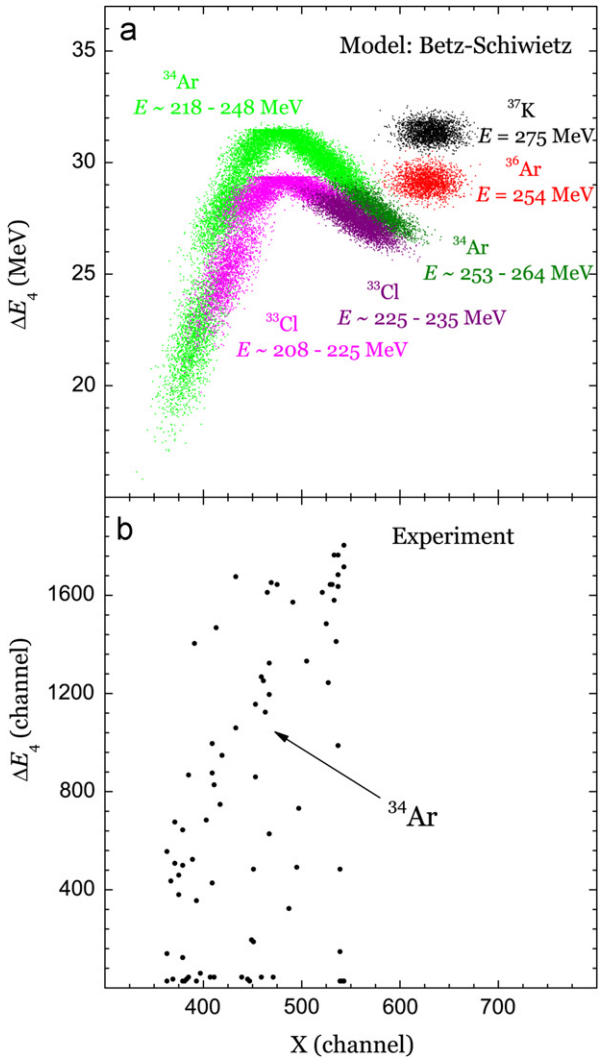

Fig. 9. (Color online) (a) Calculated two-dimensional spectrum of one of the anode strips of the ionization chamber (ΔE_4) vs X obtained using the code RAYTRACE-GFM, for the recoils of the p(^{37}K,^{34}Ar)α and p(^{36}Ar,^{33}Cl)α reactions at 275 and 254 MeV, respectively. The groups of ^{34}Ar and ^{33}Cl recoils together with the islands of ^{37}K and ^{36}Ar from elastic scattering are indicated. (b) Experimental spectrum for the same reaction. The events with $\Delta E_4 \sim 0$ are caused by particles that are stopped in various wire grids of the x–y position sensitive detector located in front of the ionization chamber.

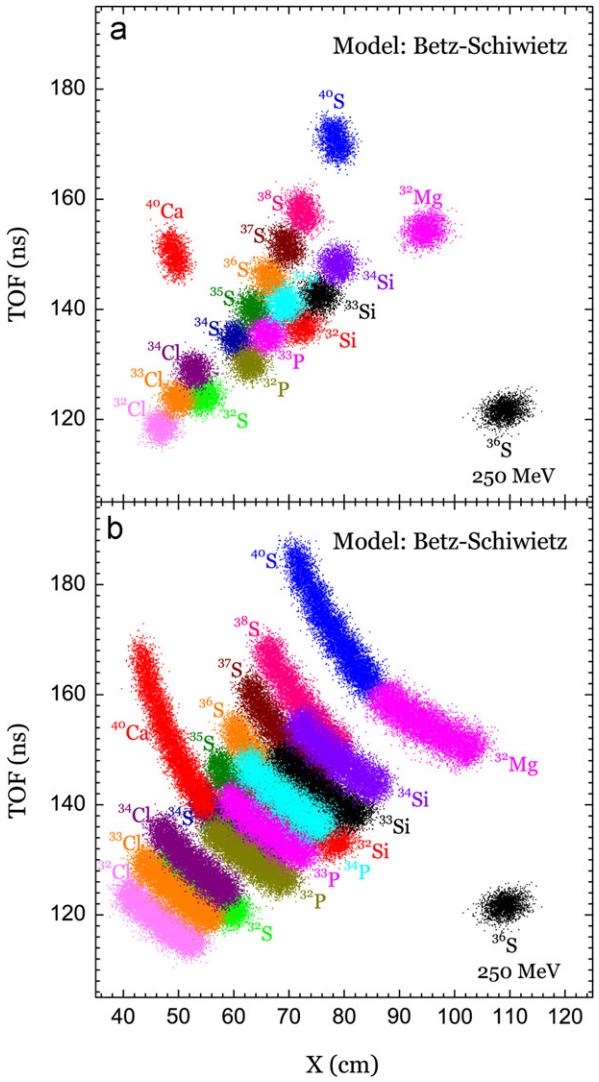

Fig. 10. (Color online) Two-dimensional TOF vs X distributions of various particle groups produced in deep-inelastic collisions of 250 MeV ^{36}S ions on a ^{208}Pb target. The reaction products are assumed to be emitted with their respective Coulomb barrier energies. The top part of Fig. 10 shows the separation of the various DIC products from the incident beam in the TOF vs X plane. This separation disappears if a velocity dispersion of ±5% is included (see bottom panel).

the TOF vs X plane expected for elastically scattered ^{36}S particles and several reaction products from deep inelastic collisions (^{32,36,40}S, ^{32}Mg and ^{40}Ca). Similar to the results obtained in our experiments (Section 3) there is a spatial separation between the lower-energy deep-inelastic reaction products and the higher-energy beam particles which can be used to reduce the count rate in a detector. On average the DIC products are separated from the scattered ^{36}S beam in the focal plane of a gas-filled split-pole spectrograph by about 40 cm. Neutron-rich low-Z isotopes (e.g., ^{32}Mg), however, have magnetic rigidities that overlap with the ^{36}S beam. Contrary to the detection of the target-like reaction products some spatial separation of the individual beam-like isotopes can be achieved. This separation for the beam-like reaction products deteriorates, however, if we take into account that the DIC reaction products are emitted with a finite energy distribution. This effect is non-negligible as shown in Fig. 10(b) where the effect of a ±5% energy distribution width on the TOF vs X distributions of Fig. 10(a) has been calculated. Additional signals from, e.g., the IC can be used to improve the separation, but simulations show that the improvement is only marginal. These results indicate, however that a GFM leads to a spatial separation of the beam and the DIC products although the separation between individual reaction products is marginal. However, since the GFM technique results in a charge-state focusing effect it can be used together with a γ detector to identify with good efficiency deep-inelastic reaction products in the focal plane of a gas-filled separator.

5. Summary

Through a series of measurements using stable and radioactive ion beams we have determined a parameterization of the average charge state $\overline{q}$ for ions moving through a magnetic field region filled with nitrogen gas which is valid in the mass $A \sim 20-40$ region. Using this parameterization in a RAYTRACE-GFM calculation we can quantitatively describe the movement of intermediate-mass ions in a gas-filled split-pole spectrograph. The ability of the

gas-filled magnet technique to separate the (p,α) reaction products from the beam particles has been established through measurements with ^{33}S and ^{37}K beams. Since the gas-filled magnet method, however, is not independent of the velocity of the ion (i.e., it is not fully velocity focusing) there can still be considerable overlap between different particle species, which limits the general application of this technique to other fields.

Acknowledgements

We want to thank the ATLAS operations staff for providing the beams used in this study. This work was supported by the US Department of Energy, Office of Nuclear Physics under contract No. DE-AC02-06CH11357, by the NSF JINA Grant No. PHY0822648 and the Consejo Nacional de Investigaciones Científicas y Técnicas (CONICET), Argentina.

References

[1] B. Harss, J.P. Greene, D. Henderson, R.V.F. Janssens, C.L. Jiang, J. Nolen, R.C. Pardo, K.E. Rehm, J.P. Schiffer, R.H. Siemssen, A.A. Sonzogni, J. Uusitalo, I. Wiedenhöver, M. Paul, T.F. Wang, F. Borasi, R.E. Segel, J.C. Blackmon, M.S. Smith, A. Chen, P. Parker, Physical Review Letters 82 (1999) 3964.
[2] A.A. Sonzogni, K.E. Rehm, I. Ahmad, F. Borasi, D.L. Bowers, F. Brumwell, J. Caggiano, C.N. Davids, J.P. Greene, B. Harss, A. Heinz, D. Henderson, R.V.F. Janssens, C.L. Jiang, G. McMichael, J. Nolen, R.C. Pardo, M. Paul, J.P. Schiffer, R.E. Segel, D. Seweryniak, R.H. Siemssen, J.W. Truran, J. Uusitalo, I. Wiedenhöver, B. Zabransky, Physical Review Letters 84 (2000) 1651.
[3] H. Schatz, K.E. Rehm, Nuclear Physics A 777 (2006) 601.
[4] A. Parikh, J. José, F. Moreno, C. Iliadis, Astrophysical Journal Supplement Series 178 (2008) 110.
[5] J.L. Fisker, H. Schatz, F.K. Thielemann, Astrophysical Journal Supplement Series 174 (2008) 261.
[6] B. Harss, R.C. Pardo, K.E. Rehm, F. Borasi, J.P. Greene, R.V.F. Janssens, C.L. Jiang, J. Nolen, M. Paul, J.P. Schiffer, R.E. Segel, J. Specht, T.F. Wang, P. Wilt, B. Zabransky, Reviews of Scientific Instruments 71 (2000) 380.
[7] C.M. Deibel, K.E. Rehm, J.M. Figueira, J.P. Greene, C.L. Jiang, B.P. Kay, H.Y. Lee, J.C. Lighthall, S.T. Marley, R.C. Pardo, N. Patel, M. Paul, C. Ugalde, A. Woodard, A.H. Wuosmaa, G. Zinkann, Physical Review C 84 (2011) 045802.
[8] C.B. Fulmer, B.L. Cohen, Physical Review 109 (1958) 94.
[9] B.L. Cohen, C.B. Fulmer, Nuclear Physics 6 (1958) 547.
[10] P. Armbruster, Nukleonik 3 (1961) 188.
[11] K. Sistemich, J.W. Grüter, H. Lawin, J. Eidens, R. Fabbri, T.A. Khan, W.D. Lauppe, G. Sadler, H.A. Selic, M. Shaanan, P. Armbruster, Nuclear Instrumentation and Methods in Physics Research 130 (1975) 491.
[12] H. Lawin, J. Eidens, J.W. Borgs, R. Fabbri, J.W. Grüter, G. Joswig, T.A. Khan, W.D. Lauppe, G. Sadler, H.A. Selic, M. Shaanan, K. Sistemich, P. Armbruster, Nuclear Instrumentation and Methods in Physics Research 137 (1976) 103.
[13] A. Ghiorso, S. Yashita, M.E. Leino, L. Frank, J. Kalnins, P. Armbruster, J.-P. Dufour, P.K. Lemmertz, Nuclear Instrumentation and Methods in Physics Research Section A 269 (1988) 192.
[14] V. Ninov, P. Armbruster, F.P. Heßberger, S. Hofmann, G. Münzenberg, Y. Fujita, M. Leino, A. Lüttgen, Nuclear Instrumentation and Methods in Physics Research Section A 357 (1995) 486.
[15] M. Leino, J. Äystö, T. Enqvist, P. Heikkinen, A. Jokinen, M. Nurmia, A. Ostrowski, W.H. Trzaska, J. Uusitalo, K. Eskola, P. Armbruster, V. Ninov, Nuclear Instrumentation and Methods in Physics Research Section B 99 (1995) 653.
[16] K. Subotic, Yu.Ts. Oganessian, V.K. Utyonkov, Yu.V. Lobanov, F.Sh. Abdullin, A.N. Polyakov, Yu.S. Tsyganov, O.V. Ivanov, Nuclear Instrumentation and Methods in Physics Research Section A 481 (2002) 71.
[17] M. Paul, B.G. Glagola, W. Henning, J.G. Keller, W. Kutschera, Z. Liu, K.E. Rehm, B. Schneck, R.H. Siemssen, Nuclear Instrumentation and Methods in Physics Research Section A 277 (1989) 418.
[18] W. Henning, W.A. Bell, P.J. Billquist, B.G. Glagola, W. Kutschera, Z. Liu, H.F. Lucas, M. Paul, K.E. Rehm, J.L. Yntema, Science 236 (1987) 725.
[19] C. Li, Y. Guan, S. Jiang, M. He, X. Ruan, W. Wang, D. Zhang, J. Yuan, S. Wu, K. Dong, Nuclear Instrumentation and Methods in Physics Research Section B 268 (2010) 876.
[20] U. Morgenstern, L.K. Fifield, S.G. Tims, R.G. Ditchburn, Nuclear Instrumentation and Methods in Physics Research Section B 268 (2010) 739.
[21] K.E. Rehm, M. Paul, J. Gehring, B. Glagola, D. Henderson, W. Kutschera, A.H. Wuosmaa, Nuclear Instrumentation and Methods in Physics Research Section A 344 (1994) 614.
[22] J.F. Liang, D. Shapira, J.R. Beene, J.D. Bierman, A. Galindo-Uribarri, J. Gomez del Campo, C.J. Gross, M.L. Halbert, T.J. Harding, A.I.D. Macnab, S.P. McNeal, R.L. Varner, K. Zhao, Nuclear Instrumentation and Methods in Physics Research Section A 435 (1999) 393.
[23] C. Schmitt, M. Rejmund, A. Navin, B. Lecornu, B. Jacquot, G. de France, A. Lemasson, A. Shrivastava, P. Greenlees, J. Uusitalo, K. Subotic, L. Gaudefroy, C. Theisen, B. Sulignano, O. Dorvaux, L. Stuttgé, Nuclear Instrumentation and Methods in Physics Research Section A 621 (2010) 558.
[24] K.E. Rehm, C.L. Jiang, M. Paul, D. Blumenthal, J. Gehring, D. Henderson, J. Nickles, J. Nolen, R.C. Pardo, A.D. Roberts, J.P. Schiffer, R.E. Segel, Nuclear Instrumentation and Methods in Physics Research Section A 370 (1996) 438.
[25] H.D. Betz, Reviews of Modern Physics 44 (1972) 465.
[26] H.D. Betz, in: S. Datz (Ed.), Applied Atomic Collision Physics, Academic Press, New York, 1983, vol. 4, p. 1.
[27] M. Paul, Nuclear Instrumentation and Methods in Physics Research B 52 (1990) 315.
[28] S. Kowalski, H.A. Enge, RAYTRACE, MIT Internal Report, 1986.
[29] S.B. Kowalski, H.A. Enge, Nuclear Instrumentation and Methods in Physics Research A 258 (1987) 407.
[30] H.D. Betz, G. Hartig, E. Leischner, C. Schmelzer, B. Stadler, J. Weihrauch, Physics Letters 22 (1966) 643.
[31] H.D. Betz, C. Schmelzer, Unilac Report 1-67, 1967, Universitat Heidelberg, unpublished.
[32] I.S. Dmitriev, V.S. Nikolaev, Zhurnal Eksperimental'noi i Teoreticheskoi Fiziki 47 (1964) 615. (English translation: Soviet Physics JETP 20 (1965) 409).
[33] G. Schiwietz, P.L. Grande, Nuclear Instrumentation and Methods in Physics Research B 175 (2001) 125.
[34] J.M. Figueira, et al., to be published.
[35] R.C. Pardo, et al., to be published.
[36] 〈http://www.gsi.de/iris10/〉.